2007 IEEE International Conference on
Robotics and Automation
Roma, Italy, 10-14 April 2007

Trajectory Control of a Four-Wheel Skid-Steering Vehicle over Soft Terrain using a Physical Interaction Model

D. Lhomme-Desages*, Ch. Grand* and J-C. Guinot*
*Laboratoire de Robotique de Paris
Route du Panorama, 92260 Fontenay-aux-Roses
lhomme@robot.jussieu.fr, grand@robot.jussieu.fr, guinot@robot.jussieu.fr

***Abstract*— A model-based control for fast autonomous four-wheel mobile robots on soft soils is developed. This control strategy takes into account slip and skid effects to extend the mobility over planar granular soils. Each wheel is independently actuated by an electric motor. The overall objective is to follow a path roughly at relatively high speed. Some results obtained in dynamic simulation are presented.**

I. INTRODUCTION

Many popular controllers for wheeled mobile robots assume that wheels roll without slipping. This leads to a nonholonomic constraint added to the kinematic or dynamic model [1]. This assumption is quite legitimate for usual applications such as autonomous cars over hard terrains or slow indoor exploration. However, it is no longer suitable for many applications where wheel slip cannot be neglected [2], especially for traveling over natural soils at high speed [3].

With this type of control architecture, the stability of the rover cannot be guaranteed in presence of slippage, due to the dynamics of the vehicle and the saturation of admissible forces by the soil. Therefore, a new control scheme is required.

In this paper, a model-based control method for fast autonomous mobile robots on soft soils is developed. On such a type of terrain (sand for instance), slip and skid phenomena may be significant. The control strategy takes into account these effects to extend the mobility of the vehicles over natural soils. The terrains considered here are horizontal and relatively smooth compared to the size of the wheels.

A non-linear model-based control of wheel slippage is studied, using a semi-empirical wheel-soil interaction model. A higher-level control is applied to a four-wheel skid-steering vehicle which can travel at relatively high speed (several meters per second). Each wheel is independently actuated by an electric motor.

The overall objective is to follow a given trajectory at relatively high speed. This controller implies a low-level control method that aims to regulate the slip rate of one wheel, since the traction force generated by the rotation of the wheel at the contact patch depends on the wheel slip. Limitations and required sensors are also pointed out.

Finally, this control scheme is evaluated in dynamic simulation. The results show an improvement of motion control when implementing the model-based traction control.

II. SYSTEM MODELLING

A. Rover model

We consider a skid-steering vehicle with four independent electrically driven wheels. The kinematic and geometric parameters of the vehicle are shown on figure 1.

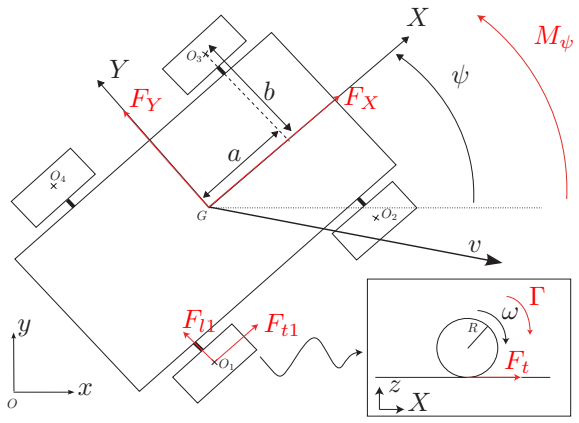

Fig. 1. Model of a four-wheel rover

The center of mass G is located at the center of the platform. See Tab. I for a description of notations. ψ is the orientation of the vehicle relatively to (O, x).

B. Wheel-soil interaction model

Several modeling frameworks can be used to calculate the forces involved in the wheel-soil interaction process. We use an extended version of the terramechanic model introduced by Bekker ([4],[5]). We assume that the entire wheel is very stiff compared to the ground and we can consider that the wheel is rigid (Fig. 2).

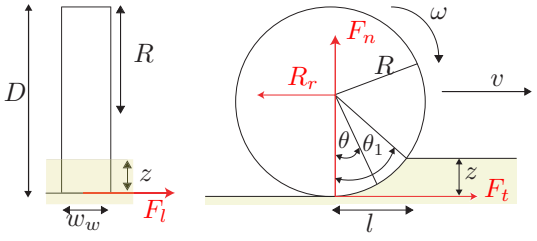

Fig. 2. Model of a rigid wheel

Denote v the velocity of the center of the wheel, and ω the angular velocity of the wheel. In this model, the traction force depends on the slip rate s, which is defined as:

$$s = \begin{cases} 1 - \frac{v}{\omega.R} & if \quad R\omega \geq v \\ 1 - \frac{\omega.R}{v} & if \quad R\omega < v \end{cases} \tag{1}$$

for $v > 0$ and $\omega > 0$. This definition can be extended to every $(v, \omega) \in \Re^2$, as is shown in Fig. 3.

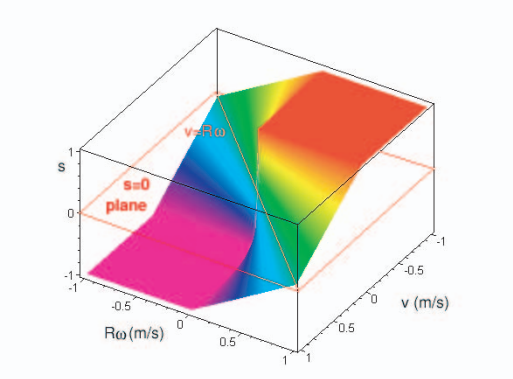

Fig. 3. Slip rate as a function of v and $R\omega$

According to Bekker theory [4], the normal force depends on the wheel sinkage z through:

$$F_n = \frac{1}{3}\left[w_w \left(\frac{k_c}{r} + k_\phi\right)(3-n)\sqrt{D} z^{\frac{2n+1}{2}}\right] \tag{2}$$

where k_c, k_ϕ and n are soil parameters. w_w is the width of the wheel.

$r = \min(w_w, l)$, l being the length of the contact patch.

The net traction force DP (also known as drawbar pull) is the difference between the raw traction force and the rolling resistance:

$$DP(s) = F_t(s) - R_r \tag{3}$$

In this study, the rolling resistance is assumed to be mainly caused by soil compaction, which allows to use the expression:

$$R_r = w_w \frac{z^{n+1}}{n+1}\left(\frac{k_c}{r} + k_\phi\right) \tag{4}$$

The raw traction force is related to the slip rate:

$$\begin{aligned} F_t(s) &= F_m\left[1 - \tfrac{K}{s.l}\left(1 - e^{-s.l/K}\right)\right] \\ F_m &= l w_w c + F_n \tan\phi \end{aligned} \tag{5}$$

where c, ϕ and K are soil cohesion, friction angle and shear deformation modulus, respectively.

The shape of F_t is plotted on Fig. 4 with parameters of Tab. I. This is a monotonic function and it reaches its extreme values $\pm F_{tmax}$ for extreme values of s.

Lateral forces can be implemented, including bulldozing resistance, as described in [6]. In this study, we use a simple linearized Coulomb model for lateral forces:

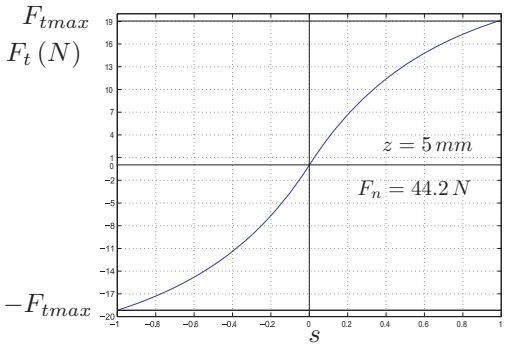

Fig. 4. Traction force vs. slip rate

$$F_l = \mu_l(d_l).F_n = \mu_{ls}\left(1 - e^{d_l/d_{ls}}\right)F_n \tag{6}$$

where d_{ls} and μ_{ls} are soil characteristics, d_l is the lateral displacement.

This contact model has been validated by experimental measurements on an instrumented testing bench (Fig. 5).

A set of experimental data is depicted in Fig. 6. A curve-fitting algorithm is used to find the soil parameters of the interaction model. The resulting curve fits relatively well the data, despite a high experimental noise of about $\pm 10\,N$.

Fig. 5. Experimental device

III. TRAJECTORY TRACKING CONTROL

The objective of this model-based control scheme is the tracking of a reference trajectory given under the form $(x^*(t), y^*(t), \psi^*(t))$.

We denote $\mathbf{F}$ the global vector of forces and torque applied to the center of mass of the platform, in the local frame attached to the chassis. This vector has two components since the lateral motion is uncontrollable: no combination of traction forces can result in a lateral motion. Therefore, the lateral component F_Y is ignored:

$$\mathbf{F} = \begin{bmatrix} F_X \\ M_\psi \end{bmatrix} \tag{7}$$

A. Control architecture

Figure 7 presents the overall control system. The role of the trajectory controller is to generate a proper desired global force $\mathbf{F}^*$. Then each raw traction force $F_t{}^*$ is computed from the global desired force by solving the forces balance. Lateral forces and rolling resistance are estimated using the

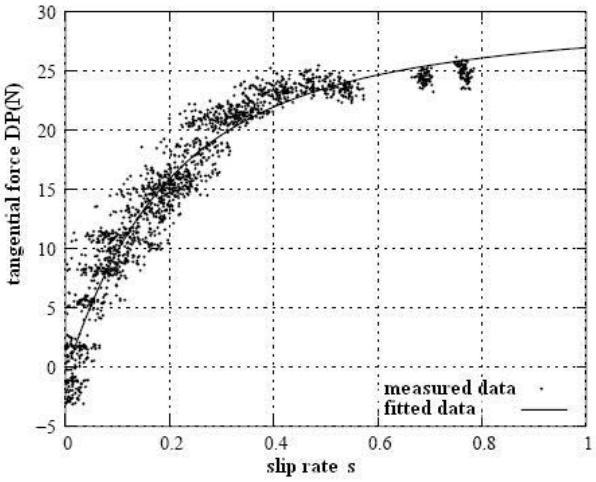

Fig. 6. Experimental measure of drawbar pull

terramechanic model. The inversion of the estimated wheel-soil contact model provides the desired slip rate s^* from ${F_t}^*$.

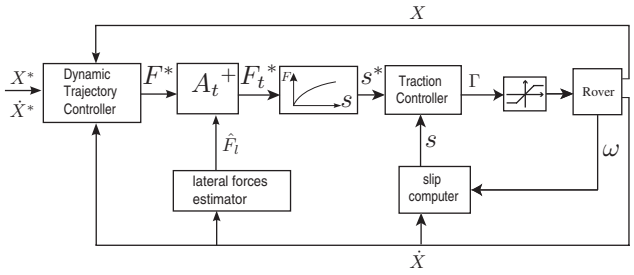

Fig. 7. Control block diagram

This architecture is composed of two stages, the trajectory control and the traction control, which are detailed in the next sections. The traction controller regulates the slip rate of each wheel.

The input desired torques are saturated to ensure that desired values do not exceed actuators capabilites.

B. Trajectory controller

The trajectory controller is a high-level module that generates a desired $\mathbf{F}^*$ corresponding to a desired motion of the robot toward the desired trajectory (Fig. 8). The desired global force depends on the kinematic and geometric situation ($\mathbf{F}^* = f(\mathbf{X}, \dot{\mathbf{X}})$).

Note d the distance between the platform center of mass and the desired reference position.

Define the errors in velocity and heading angle:

$$e_v = v^* - v \tag{8}$$

$$e_\psi = \tilde{\psi} - \psi \tag{9}$$

Instead of the reference angle $\psi^*(t)$ of the reference trajectory, the desired angle is:

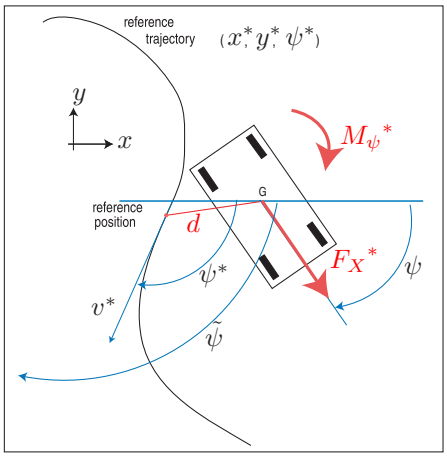

Fig. 8. Parameters for the trajectory control

$$\tilde{\psi}(d) = \psi^* - \arctan(k_f d) \tag{10}$$

This defines a modified reference angle that depends also on the distance d. k_f is a tuning parameter. Equation (10) is intended to reduce the distance to the reference trajectory even with a passive lateral motion.

A simple strategy may be defined as the following:

$${F_X}^* = k_{pX} e_v + k_{iX} \int e_v \tag{11}$$

$${M_\psi}^* = k_{p\psi} e_\psi + k_{i\psi} \int e_\psi + k_{d\psi} \dot{e_\psi} \tag{12}$$

where k_{iX}, k_{pX}, $k_{p\psi}$, $k_{i\psi}$ and $k_{d\psi}$ are gains. This defines a PI-controller on operational velocity v and a PID-control of the heading angle ψ.

C. Tractive force distribution

Each wheel is subjected to tangential lateral and longitudinal contact forces, gathered in corresponding vectors:

$$\mathbf{F_t} = [DP_1, DP_2, DP_3, DP_4]^T \tag{13}$$

$$\mathbf{F_l} = [F_{l1}, F_{l2}, F_{l3}, F_{l4}]^T \tag{14}$$

The position of the robot is the position of the platform center of mass in the referential frame:

$$\mathbf{X} = [x, y, \psi]^T \tag{15}$$

and $\boldsymbol{\omega}$ is the vector of angular velocities of the wheels.

For each wheel, we can separate the contributions of lateral and longitudinal forces, which are related to the global force by a linear equation:

$$\mathbf{F} = \mathbf{A_t F_t}\left(\dot{\mathbf{X}}, \boldsymbol{\omega}\right) + \mathbf{A_l F_l}\left(\dot{\mathbf{X}}\right) \tag{16}$$

with:

$$\mathbf{A}_t = \begin{bmatrix} 1 & 1 & 1 & 1 \\ b & b & -b & -b \end{bmatrix} \tag{17}$$

$$\mathbf{A}_l = \begin{bmatrix} 0 & 0 & 0 & 0 \\ -a & a & a & -a \end{bmatrix} \quad (18)$$

Therefore, assuming translation and angular velocities are known, we can deduce the longitudinal forces to apply. Angular velocities can be easily measured via optical encoders. Ground velocity can be estimated using a Doppler sensor for instance [7].

We can inverse the linear system (16) by minimizing the 2-norm of vector $\mathbf{Ft}$ (thus minimizing tractive efforts). Using the pseudo-inverse of $\mathbf{A_t}$, the optimal tractive efforts are computed from equation (19), where hats denote estimated values, and stars denote desired values:

$$\mathbf{F_t}^* = \mathbf{A_t}^+ \left(\mathbf{F}^* - \mathbf{A_l}\widehat{\mathbf{F_l}} \right) \quad (19)$$

The pseudo-inverse of this matrix $\mathbf{A_t}$ can be symbolically solved:

$$\mathbf{A_t}^+ = \frac{1}{4b} \begin{bmatrix} b & 1 \\ b & 1 \\ b & -1 \\ b & -1 \end{bmatrix} \quad (20)$$

D. Model-based traction control

In order to apply motor torques corresponding to desired traction efforts, the interaction contact model is used to take into account the capabilities of the ground.

The forces balance equation gives the desired net traction force DP for each wheel. Using the Bekker-Wong model described in section II, the rolling resistance is first estimated from eq. (4). To perform this estimation, an estimation of the sinkage z is calculated on the basis of eq. (2). Normal forces F_{ni} are assumed to be equal to the fourth of the total weight:

$$F_{ni} = (m_c + 4m_r)g/4, \;\; 1 \leq i \leq 4 \quad (21)$$

This strong assumption means that the center of mass is located at the center of the platform and that there is no lateral or longitudinal load transfers.

Then, the raw traction force F_t is computed using eq. (3). Finally, the $F_t\,(s)$ function (eq. (5)) can be inversed to obtain a desired slip rate.

The tractive efforts can be unreachable if we consider the contact model. If the desired force is not admissible by the soil ($|F_t| > F_{tmax}$, i.e. $|s| = 1$), then the robot will be unable to follow the path with accuracy and will skid.

The lateral efforts $\widehat{\mathbf{F_l}}$ are estimated with the lateral contact model and a measure of the kinematic state of the vehicle.

E. Slip servoing

Several slip control methods exist in the literature, including nonlinear and gain-scheduled PID, sliding mode [8], fuzzy logic [9], or Lyapunov synthesis [10].

Simple slip control strategies have been used for several mobile robots in rough terrain ([11], [12]). Like these authors, we implement a simple PI-controller (Fig. 9). A derivative gain is inappropriate since the slip rate is a discontinuous function. Each independent electric motor is controlled in torque (namely in current).

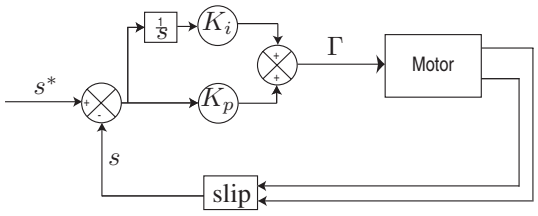

Fig. 9. Control block diagram with PI-controller

Numerical simulations of a one-wheel vehicle have been led in a dynamical multibody modeling software [13]. An extension to this software has been developed to implement the terramechanic contact model. The step response of the controller is depicted on Fig. 10 ($s^* = 0.8$, $K_p = K_i = 100$).

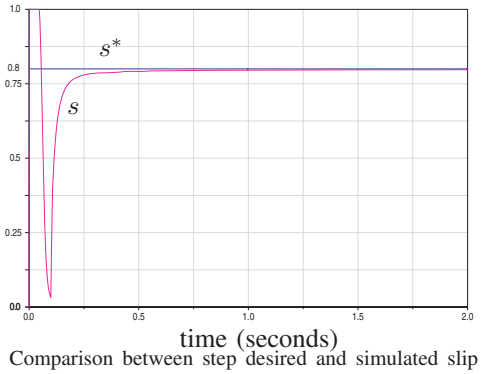

Fig. 10. Comparison between step desired and simulated slip rate with PI-control

After a short period where s is not continuous (at $t = 0^+$, $v = 0$ and $\omega > 0$, see Fig. 3), it converges toward the desired value.

IV. SIMULATION RESULTS

To simulate the behavior of the robot, a simple desired maneuver has been chosen, which is a right bend at constant desired tangential velocity (1.7 m/s) after an acceleration phase at constant rate. The minimal radius of curvature is 54 cm. Kinematic, dynamical and contact parameters are given in the table I. Soil parameters correspond to a dry sandy soil [5]. Dynamic and geometrical parameters are those of a project of a testing skid-steering platform.

A passive revolute joint has been introduced between both sides of the platform to guarantee an isostatic contact.

A. Trajectory control without traction control

In order to test and validate the traction control, a simulation is made without the model-based traction control subsystem. Therefore, the contact model is not involved in the control architecture and the lateral forces are ignored, which means they are processed as perturbations. Since the contact model is not used, the rolling resistance is also ignored, so it is implicitly assumed that $F_t = DP$ for each wheel.

In this case, the distribution of the global desired force is:

TABLE I

SIMULATION PARAMETERS

m_r	$1\,kg$	wheel mass
m_c	$14\,kg$	chassis mass
J	$1.03.10^{-2}\,kg.m^2$	wheel inertia
R	$10\,cm$	wheel radius
w_w	$6\,cm$	wheel width
a	$35\,cm$	half wheelbase
b	$23\,cm$	half track width
n	0.705	soil exponent
k_c	$6940\ N.m^{-(n+1)}$	cohesive modulus
k_ϕ	$505800\ N.m^{-(n+2)}$	friction modulus
ϕ	31.5 deg	friction angle
c	$1150\,Pa$	cohesion
K	$1.15\,cm$	soil modulus
K_p	300	proportional gain for slip servoing
K_i	1000	integral gain for slip servoing

$$\mathbf{F_t}^* = \mathbf{A_t}^+ \mathbf{F}^* \tag{22}$$

For each wheel, the desired traction force F_t^* is directly translated to a torque using:

$$\Gamma = RF_t^* \tag{23}$$

The inertial term of the dynamic equation of the wheel motion is ignored, as well as the soil capabilities. The resulting control architecture is represented on Fig. 11.

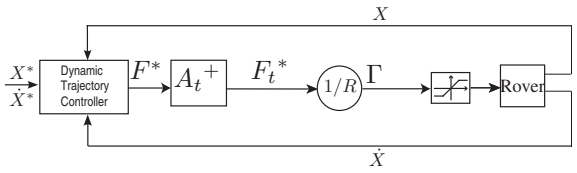

Fig. 11. Control block diagram

The simulation gives the sequence shown in Fig. 12.

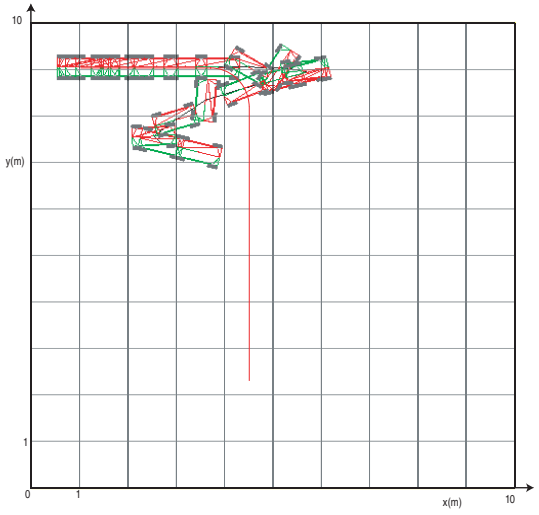

Fig. 12. Trace of the motion of the rover

The unstable behavior of the system is clearly highlighted.

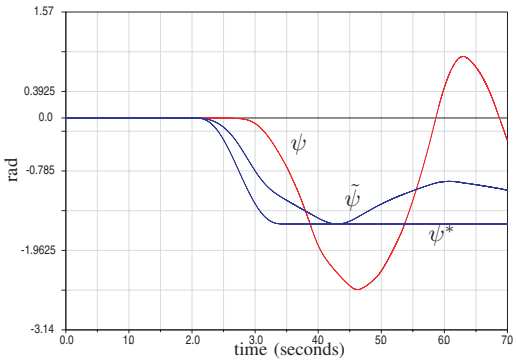

Fig. 13. Rover direction and desired heading angle

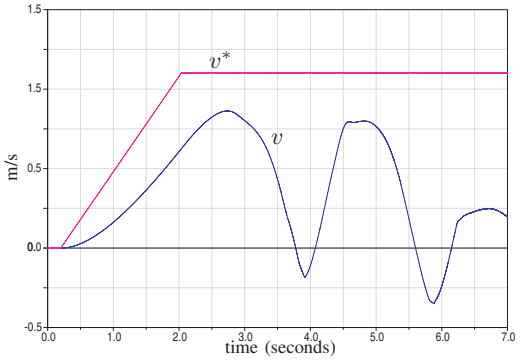

Fig. 14. Rover velocity

It can be seen from Fig. 15 that the slip rate reaches its maximum (soil failure regions). The ground cannot admit traction forces that are required to stabilize the system.

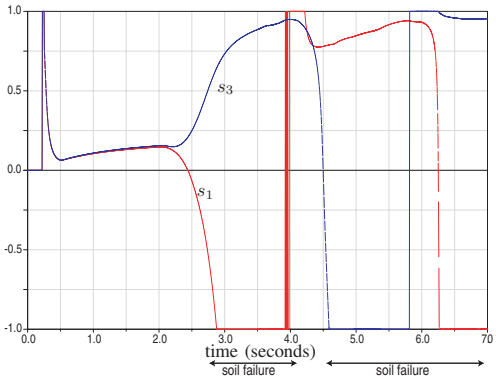

Fig. 15. Slip rates

For this particular set of parameters and gains, the system is unstable. More generally, the control of this type of autonomous robots in presence of large slip is problematic.

B. Model-based Trajectory control

With the implementation of the control architecture developed in this paper, we obtain the sequence of the figure 16. Despite the lack of accuracy of the tracking, which is sec-

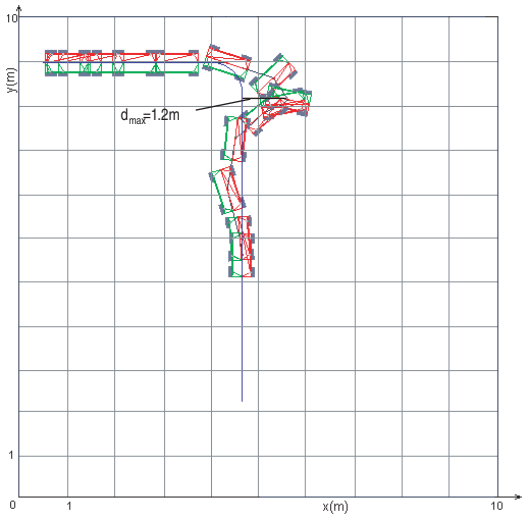

Fig. 16. Trace of the motion of the rover

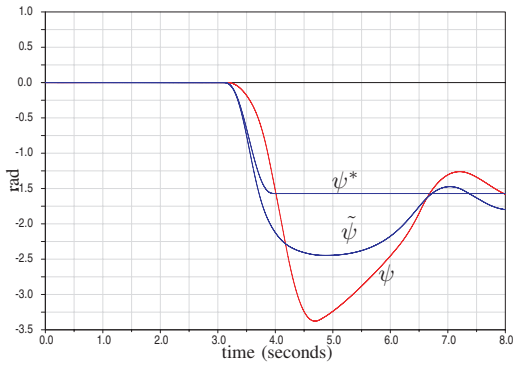

Fig. 17. Rover direction and desired heading angle

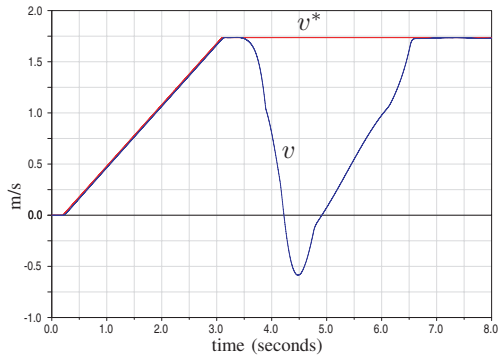

Fig. 18. Rover velocity

ondary for high-speed applications, the control architecture allows the stability of the system.

The figure 18 shows that the tangeantial velocity can be negative, which is acceptable, but very inefficient for power consumption.

These results show that the trajectory tracking is improved under such conditions with the model-based control scheme developed in section III .

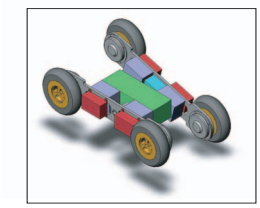

Fig. 19. Skid-steering demonstrator

V. CONCLUSION AND FUTURE WORKS

The controller presented in this paper may be useful to achieve better performances on challenging terrains such as planetary surfaces, but requires a larger instrumentation. In particular, this model-based control may be used for obstacle avoidance at high speed.

Further works are being made to implement this control strategy in a fast mobile robotic platform under development (Fig. 19). Absolute ground velocity will be measured with a Doppler radar sensor. Robustness and sensitivity to soil parameters have to be evaluated. If the algorithm is robust enough, then a real-time nonlinear estimation of contact parameters is not required as long as the terrain is relatively homogeneous. An off-line initialization procedure may be suitable.

REFERENCES

[1] L. Caracciolo, A. De Luca, and S. Iannitti, "Trajectory tracking control of a four-wheel differentially driven mobile robot," in *Proc. IEEE Intl Conf. on Robotics & Automation*, Detroit, USA, May 1999, pp. 2632–2638.

[2] T. Huntsberger, H. Aghazarian, Y. Cheng, E. Baumgartner, E. Tunstel, C. Leger, A. Trebi-Ollennu, and P. S. Schenker, "Rover autonomy for long range navigation and science data acquisition on planetary surfaces," in *Proc. IEEE Intl Conf. on Robotics & Automation*, Washington DC, USA, May 2002, pp. 3161–3168.

[3] M. Spenko, K. Iagnemma, and S. Dubowsky, "High speed hazard avoidance for mobile robots in rough terrain," in *SPIE Conf. on Unmanned Ground Vehicles*, 2004.

[4] M. Bekker, *Introduction to Terrains-Vehicles Systems*. The University of Michigan Press, 1969.

[5] J. Y. Wong, *Terramechanics and Off-Road Vehicles*. Elsevier, 1989.

[6] G. Ishigami, A. Miwa, and K. Yoshida, "Steering trajectory analysis of planetary exploration rovers based on all-wheel dynamics model," in *8th Intl Symposium on Artifical Intelligence, Robotics and Automation in Space*, Munich, Germany, Sept. 2005.

[7] S. Stuchly, A. Thansandote, J. Mladek, and J. Townsend, "A doppler radar velocity meter for agricultural tractors," *IEEE Trans. Veh. Technol.*, vol. 27, no. 1, pp. 24–30, Feb. 1978.

[8] K. Buckholtz, "Reference input wheel slip tracking using sliding mode control," in *SAE World Congress Detroit*, Society of Automotive Engineers. SAE, Mar. 2002.

[9] F. Yu, J.-Z. Feng, and J. Li, "A fuzzy logic controller design for vehicle abs with a on-line optimized target wheel slip ratio," *Intl Journal of Automotive Technology*, vol. 3, no. 4, pp. 165–170, 2002.

[10] J. Kalkkuhl, T. Johansen, and J. Ludemann, "Improved transient performance of nonlinear adaptive backstepping using estimator resetting based on multiple models," *IEEE Trans. Automat. Contr.*, vol. 47, pp. 136–140, 2002.

[11] K. Yoshida and H. Hamano, "Motion dynamics of a rover with slip-based traction model," in *Proc. IEEE Intl Conf. on Robotics & Automation*, Washington, DC, USA, May 2002, pp. 3155–3160.

[12] D. Caltabiano, D. Ciancitto, and G. Muscato, "Experimental results on a traction control algorithm for mobile robots in volcano environment," in *Proc. IEEE Intl Conf. on Robotics & Automation*, New Orleans, USA, Apr. 2004, pp. 4375–4380.

[13] Msc adams. [Online]. Available: www.mscsoftware.com/products